



Article

Design and Performance of a Low-Energy Gamma-Ray Trigger System for HERD

Luis Fariña ^{*} , Keerthana Lathika, Giulio Lucchetta , Monong Yu, Joan Boix , Laia Cardiel-Sas , Oscar Blanch , Manel Martinez and Javier Rico on behalf of the HERD Collaboration [†]

Institut de Física d'Altes Energies (IFAE), The Barcelona Institute of Science and Technology (BIST), 08193 Bellaterra, Barcelona, Spain; klathika@ifae.es (K.L.); glucchetta@ifae.es (G.L.); myu@ifae.es (M.Y.); jboix@ifae.es (J.B.); laia@ifae.es (L.C.-S.); blanch@ifae.es (O.B.); martinez@ifae.es (M.M.); jrico@ifae.es (J.R.)

^{*} Correspondence: lfarina@ifae.es

[†] The full author list is included in the Appendix A.

Abstract: The High Energy cosmic-Radiation Detection (HERD) facility has been proposed as one of the main experiments on board the Chinese space station. HERD is scheduled to be installed around 2027 and to operate for at least 10 years. Its main scientific goals are the study of the cosmic ray spectrum and composition up to the PeV energy range, indirect dark matter detection, and all-sky gamma-ray observation above 100 MeV. HERD features a novel design in order to optimize its acceptance per weight, with a central 3D imaging calorimeter surrounded on top and on its four lateral sides by complementary subdetectors. A dedicated trigger, dubbed the ultra-low-energy gamma-ray (ULEG) trigger, is required to enable the detection of gamma rays down to ~ 100 MeV. The ULEG trigger design is based upon the search for energy deposition patterns on the tracker and the anticoincidence shield, compatible with the conversion of a gamma ray within the tracker volume and resulting in enough tracker hits to allow for a good-quality gamma-ray direction reconstruction. We describe the current status of the design of the ULEG trigger system. We also characterize its performance in detecting gamma rays as inferred from Monte Carlo studies.

Keywords: HERD; trigger; gamma rays



Citation: Fariña, L.; Lathika, K.; Lucchetta, G.; Yu, M.; Boix, J.; Cardiel-Sas, L.; Blanch, O.; Martinez, M.; Rico, J., on behalf of the HERD Collaboration. Design and Performance of a Low-Energy Gamma-Ray Trigger System for HERD. *Instruments* **2024**, *8*, 31. <https://doi.org/10.3390/instruments8020031>

Academic Editors: Matteo Duranti and Valerio Vagelli

Received: 6 February 2024

Revised: 23 April 2024

Accepted: 26 April 2024

Published: 4 May 2024



Copyright: © 2024 by the authors. Licensee MDPI, Basel, Switzerland. This article is an open access article distributed under the terms and conditions of the Creative Commons Attribution (CC BY) license (<https://creativecommons.org/licenses/by/4.0/>).

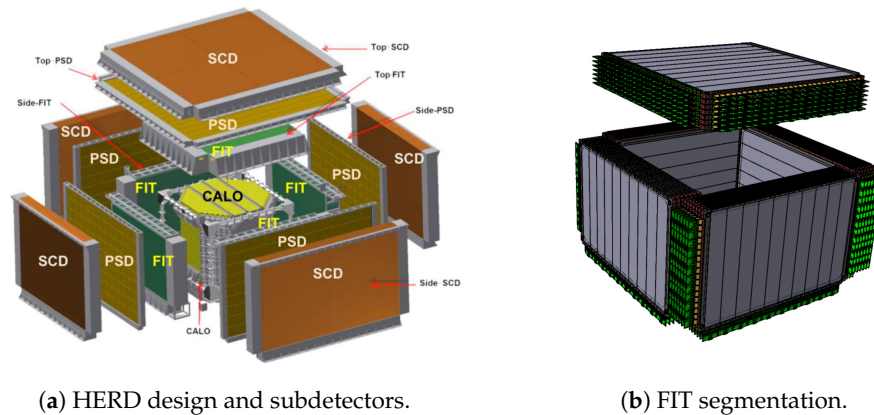
1. Introduction

The High Energy cosmic-Radiation Detection (HERD) facility is a future detector of charged cosmic rays and gamma rays scheduled to be installed aboard the Chinese space station. The experiment will begin operations around 2027, and will run for at least 10 years. As a cosmic ray detector, it aims to produce detailed spectra of the different cosmic ray species up to the knee energies and to search for dark matter signatures in these spectra. As a gamma ray detector, it will monitor the whole gamma-ray sky thanks to its unprecedented field of view [1].

HERD is designed as a multi-directional detector in order to efficiently utilize its mass budget (see Figure 1b). At its center lies a 3D-segmented calorimeter (CALO) surrounded by the rest of the subdetectors which are arranged in five active faces. From the inside out, HERD features a fiber tracker (FIT) for track reconstruction, a plastic scintillation detector (PSD) used for gamma identification and charge reconstruction, and a silicon charge detector (SCD) that provides precise charge reconstruction. On one of the lateral faces, a transition radiation detector will be used to calibrate the CALO.

The FIT (see also Figure 1a) is divided into five sectors, each covering one face of the cube. Each of these sectors consists of several layers of scintillating fibers, spanning the whole length of the side they are on. These layers are arranged in tracking pairs or double layers, with the fibers in adjacent layers running in perpendicular directions, forming a total of seven double layers. Each individual layer is segmented into modules, each containing a fiber mat and its readout. In our reference geometry, modules are ~ 10 cm

wide, each of them producing a signal that can be used for triggering. The top face contains 12 modules in every layer, while the lateral faces contain, in alternating layers, 10 vertical and 8 horizontal modules.



(a) HERD design and subdetectors.
Figure 1. HERD and FIT models.

(b) FIT segmentation.

As for the PSD, we consider a reference geometry where it consists of two staggered layers of scintillating square tiles of size $10 \times 10 \text{ cm}^2$. The top face contains 14×14 tiles, and each of the lateral faces contain 13×9 tiles. Each of these tiles is read out individually, and they produce a signal that can be used by the different triggers.

Since HERD aims to measure the fluxes of various species of cosmic ray particles, it features a set of triggers specifically designed for different particle species and energy ranges [2]. Among them, HERD includes a baseline trigger for gamma rays above $\sim 500 \text{ MeV}$, requiring a certain energy deposition in the CALO plus a combination of signals from other subdetectors. We know that HERD is sensitive to gamma rays down to the few-tens-of-MeV range (ultra-low-energy gamma, ULEG, rays) [3], but in the Low Earth Orbit, where the HERD will operate, gamma rays are outnumbered by charged particles by up to five orders of magnitude. Lowering the energy deposition threshold at the CALO would rapidly saturate its readout, so a different approach is needed.

The trigger systems in previous generations of pair-production gamma-ray space detectors operate under the designs similar to each other: first, a trigger signal is produced when a group of hits appears in spatial/temporal coincidence. Dependence on patterns containing several hits prevents triggering by noise and allows for preselecting the direction of the primary particle. For this purpose, a specific subdetector can be used (in EGRET, two layers of scintillating material are placed above and below the tracker for this purpose), or the tracker itself can be used (this is the case for AGILE, which requires hits in three out of four possible in adjacent double layers, and also in Fermi-LAT, where the main trigger condition requires hits in three adjacent double layers). In order to reject charged primaries, an additional subdetector is used (the anticoincidence shield), which must show no hits, consistently with the primary being neutral, and converting only afterwards. In both AGILE and Fermi-LAT, this subdetector is segmented into smaller elements, and information from the spatial location of the triggering hits is used to constrain a region of interest to be checked instead of the whole subdetector. Finally, the calorimeter can be checked to verify that the shower intersects it, if needed, and then instrument can be read out and the information on the event's interactions saved.

The ULEG trigger is designed in these three stages:

- Level 0 (L0): initial information of patterns of three aligned FIT modules (three-in-a-row (3IR) patterns), and of PSD elements hit by the shower.
- Level 1 (L1): the PSD information is checked against the region(s) of interest defined by the triggered elements in the FIT.
- Level 2 (L2): the energy deposited in the CALO is checked. In this study, we consider a threshold at 100 MeV .

It is important to understand the rates at which the individual elements of HERD's subdetectors are activated and the rates at which these L0, L1, and L2 signals are produced in order to ensure that the readouts do not saturate. The limiting factor is the CALO readout, which can operate at about 800 Hz [4]. However, the ULEG trigger needs to coexist with the others without hindering the achievement of HERD's scientific goals, so its rate should be well below this number.

In this study, our goal is to develop and optimize the design of the ULEG trigger, considering its efficiency on the target sample of gamma rays and its trigger rate under realistic environmental conditions.

2. Materials and Methods

2.1. Monte Carlo Simulations

The response of the detector to incident particles is simulated with the help of HerdSoftware, a framework for simulation and data analysis, which contains HERD-specific detector models and analysis algorithms. Particle generation and interactions with the detector volumes are simulated using GGS ("Generic Géant4 Simulation", [5]), a package used to carry out fast simulations with Géant4 [6]. The body of the space station is not physically simulated due to its computational complexity; instead, a volume approximating its shape is used as an exclusion region. The simulation of the detector response to these interactions is carried out using a custom EventAnalysis code available in HerdSoftware.

The goal is to study the performance of the ULEG trigger under different metrics, specifically the gamma-ray detection efficiency, and the trigger rates at different trigger levels and of different designs. The trigger rate for a given species of particle can be calculated as a convolution of its flux $\Phi(E, \theta, \phi)$ and trigger acceptance:

$$\frac{dN}{dt} = \int \frac{d^2\Phi(E, \theta, \phi)}{d\Omega dE} A_{\text{eff}}(E, \theta, \phi) d\Omega dE, \quad (1)$$

where $A_{\text{eff}}(E, \theta, \phi)$ is the effective area which can be estimated with a Monte Carlo study from

$$A_{\text{eff}}(E, \theta, \phi) = S_{\text{gen}}(\theta, \phi) \frac{N_{\text{sel}}(E, \theta, \phi)}{N_{\text{gen}}(E, \theta, \phi)}, \quad (2)$$

where $S_{\text{gen}}(\theta, \phi)$ is the generating surface perpendicular to the (θ, ϕ) direction and $N_{(\text{gen}, \text{sel})}$ refer, respectively, to the number of particles generated and to the number of particles that pass the selection cuts.

For this study, the samples of primary particles for the Monte Carlo study consist of 10^7 events per species detailed (namely protons, electrons, positrons, and alpha particles—fluxes of other particle species are negligible), generated with isotropic spatial distribution and log-uniform energy distribution between 1 MeV and 100 GeV. We consider the expected fluxes at their highest, i.e., at the highest geomagnetic latitudes seen by HERD, as reconstructed from various models and empirical data from previous missions (NINA-2, AMS-01, PAMELA, MARYA, see [7]). We assume that fluxes are independent of pointing direction except from the change at the Earth's limb, located at a polar angle of $\sim 108.3^\circ$ at the orbital altitude of HERD (above the Earth's limb the fluxes contain primary and secondary cosmic rays; below, there are only secondaries). In particular, we do not consider any smoothing of this boundary, nor do we consider any azimuthal dependence in the arrival direction of charged particles.

For the case of testing the trigger efficiency on gamma rays, we define a fiducial sample of gamma rays as the subset of gamma rays that

- travel downwards, i.e., up to 90° from the zenith,
- do not interact with the detector (namely they do not comptonize) before undergoing pair conversion,
- convert within the FIT,

- after conversion, both the electron and the positron produce hits or interactions in at least three consecutive FIT double layers in both tracking directions within each double layer (for a total of at least six hits), and
- the total energy deposited in the CALO is at least half of that of the primary.

These conditions are chosen as an approximate parametrization of the set of gamma rays that can be distinguishable from cosmic rays and the albedo background gamma rays, and for which adequate track reconstruction and energy resolution can be obtained.

2.2. Three-in-a-Row Trigger Design

The ULEG trigger is based on the same three-in-a-row concept implemented in Fermi-LAT [8]. To produce a valid trigger signal, an event must produce at least three hits in consecutive FIT double layers, and in both tracking directions within each double layer. This responds to a minimal prerequisite for acceptable track reconstruction of the gamma-ray's direction.

In Fermi-LAT, the tracker is segmented into an array of 4×4 towers, each producing independent triggers. HERD's tracker is more finely segmented (10 cm wide modules to Fermi's $40 \times 40 \text{ cm}^2$ tower-like modules). Additionally, because of its 5-face design, the normal geometrical cross-section of the FIT is larger than that of the CALO, and so the edges of the tracker are involved only for particles with off-axis incidence angles. Thus, a significant fraction of the particles of interest interacts with three fiber modules that are not vertically aligned. For this reason, we also allow trigger patterns that end in modules adjacent to the first one, as long as they pass through either of the two modules between them (see Figure 2).

This extra degree of freedom in the trigger pattern causes the inclusion of some patterns that actually decrease trigger performance, as they increase the trigger rate and/or the complexity of the trigger, without meaningful marginal increases to its scientific performance. Therefore, we remove these patterns from the trigger design. They are:

- non-CALO-intersecting: the geometric cross-section of the tracker is larger than that of the calorimeter. Some groups of 3 modules, located near the edges of the tracker, trigger primarily in events in which the shower is directed away from the calorimeter. The only information available in these cases comes from the shower development in the tracker, leading to poor energy reconstruction.
- upwards-pointing: in the lateral faces, some patterns respond primarily to particles travelling upwards, from the direction of the Earth.

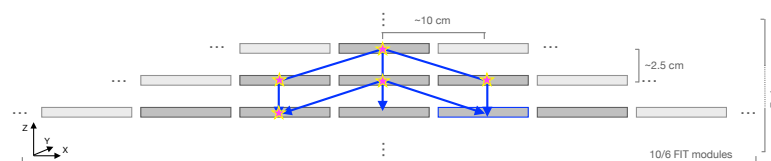


Figure 2. Schematic view of the 3IR trigger patterns.

2.3. Veto Design

At Level 1, the ULEG trigger cross-references the signals from the FIT 3IR and the PSD, producing the PSD-vetoed signals. Here, we present the performance of this veto strategy when checking the whole PSD, both as a baseline and as the simplest possible implementation. This incurs a significant loss of efficiency at high energy due to vetoing on the backsplashed part of the shower, which could be mitigated by adopting a strategy where the 3IR pattern is used to restrict the PSD elements that can produce a veto to those within a given region of interest.

3. Results

3.1. Individual Element Activation Rates

Every element capable of producing a signal relevant to the trigger is simulated independently, so Equations (1) and (2) can be applied not just to the different trigger conditions, but also to the activation of each of the individual sensitive elements that generate the signals used in the ULEG (the PSD tiles and the FIT mats). Since the sizes, shapes, location and numbers of these elements are subject to some modification as the design of the detector is finalized, we report here the activation rates per element per unit area.

We find that the activation rate of the individual elements is highly dependent on their location within HERD. An example is provided in Figure 3 for the case of the PSD. The outer layer is more exposed than the inner one due to the flux of ~ 1 MeV particles that do not penetrate to the deeper parts of the detector. In the inner layer, some elements are partially uncovered due to the staggering of the two layers and have activation rates similar to those of the outer layer. On the other hand, higher energy particles (above ~ 1 GeV) produce more interactions in the deeper layers due to increased backscplash and are responsible for the hotspot at the center of the top face, where the CALO is located. Shadowing due to the body of the space station causes the top face to be less exposed than the lateral faces, and in the latter it causes the rates to decrease as the elements move closer to the space station mount.

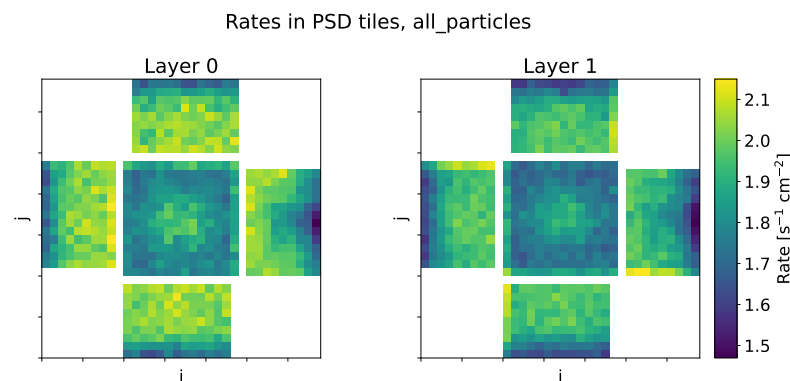


Figure 3. Estimated total activation rates of the individual tiles for the outer (0, left) and inner (1, right) layers of the PSD. Each of the pixels represents a single PSD tile. The five sections in each plot correspond to the five faces of HERD: at the center is the top face, and from the right and in counterclockwise order the other faces are designated $X+$, $Y+$, $X-$, $Y-$, and they are aligned with the space station directions forward, port, aft, and starboard, respectively. In this representation, the lateral faces are rotated so that the pixels closer to the top face correspond to the upper part of the face they are on.

According to our simulations, the activation rates are $\sim 2.2 \text{ cm}^{-2}\text{s}^{-1}$ and $\sim 1.7 \text{ cm}^{-2}\text{s}^{-1}$ for the most exposed PSD tile and FIT module. The flux models considered have large uncertainties for energies below ~ 10 MeV due to the lack of precise measurements; for the estimated worst-case-scenario (higher flux) model, the activation rates could be as high as $\sim 5.2 \text{ cm}^{-2}\text{s}^{-1}$ and $\sim 3.5 \text{ cm}^{-2}\text{s}^{-1}$, respectively, about a factor two higher. The increase is higher for the PSD, as it is the outermost detector involved in the ULEG and these particles have low penetrative power.

3.2. Trigger Performance and Rates

The total estimated trigger rates for the studied detector geometry are $\sim 2.6 \cdot 10^4 \text{ s}^{-1}$, $\sim 2 \cdot 10^2 \text{ s}^{-1}$, and $\sim 60 \text{ s}^{-1}$ for 3IR, L1 and L2, respectively (see Figure 4). The bulk of the trigger rate at L1 and L2 corresponds to events that pass along directions corresponding to the edges of the detector (see Figure 5), which indicates that this number is affected by inaccuracies in the description of HERD used for the simulations. Note that here, we

consider only the limited information available at the speed at which the triggers have to operate. L2 events are still susceptible to further cleaning after the data are stored. In the offline analysis, more information is available, including, e.g., the full resolution of the FIT (the trigger uses only mat-level resolution) and supplementary vetoing with subdetectors outside the PSD.

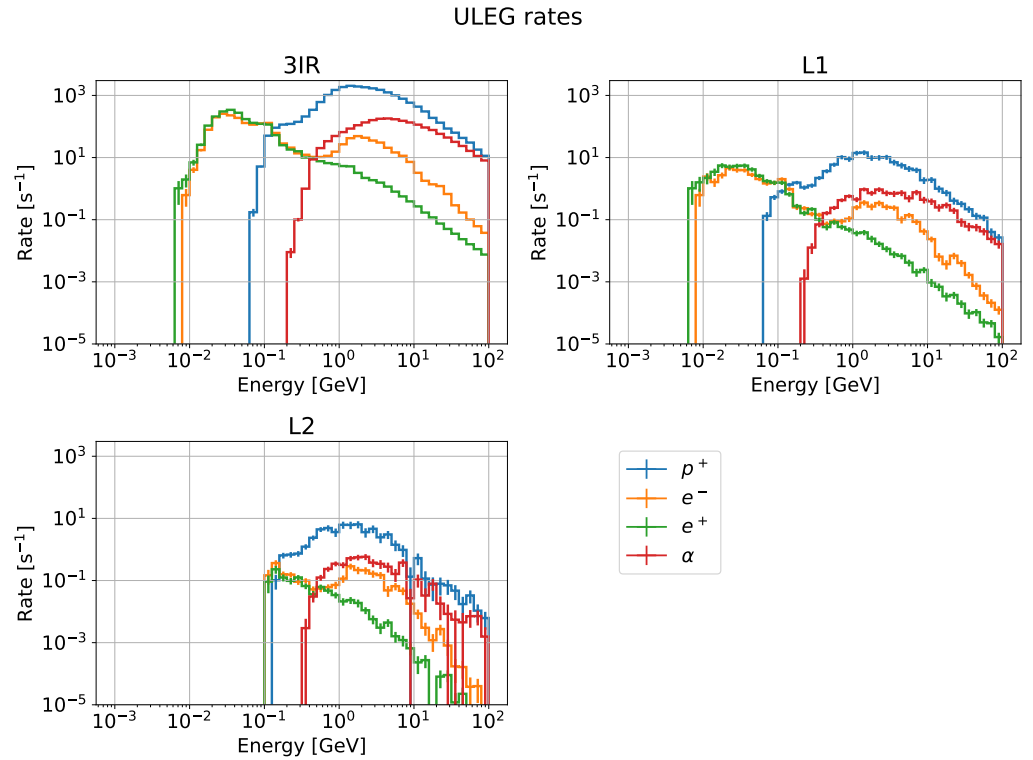


Figure 4. Expected particle rates for the different backgrounds under study and for ULEG trigger levels 3IR, L1 and L2.

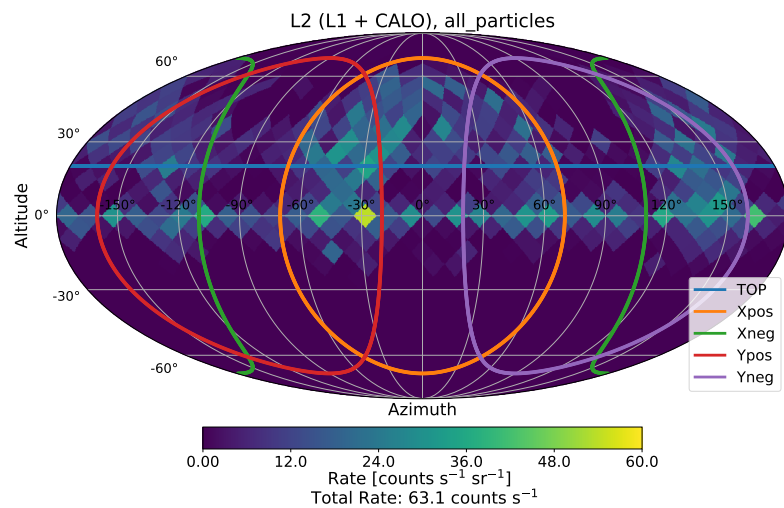


Figure 5. L2 trigger rates according to the direction of the primary as seen from HERD. The boundary of a putative 70° field of view is drawn for each face as a visual aid. Note that the boundary of the top face’s field of view is a circle corresponding to the 20° N parallel.

In order to estimate the contribution from background events that are physically indistinguishable from gamma rays, we also consider a model of HERD with a completely hermetic PSD, finding an irreducible rate of $\sim 0.2 \text{ s}^{-1}$ background events comparable to the

expected rates from the averaged galactic diffuse gamma-ray background (see Figure 6), which is the dominant gamma-ray diffuse background.

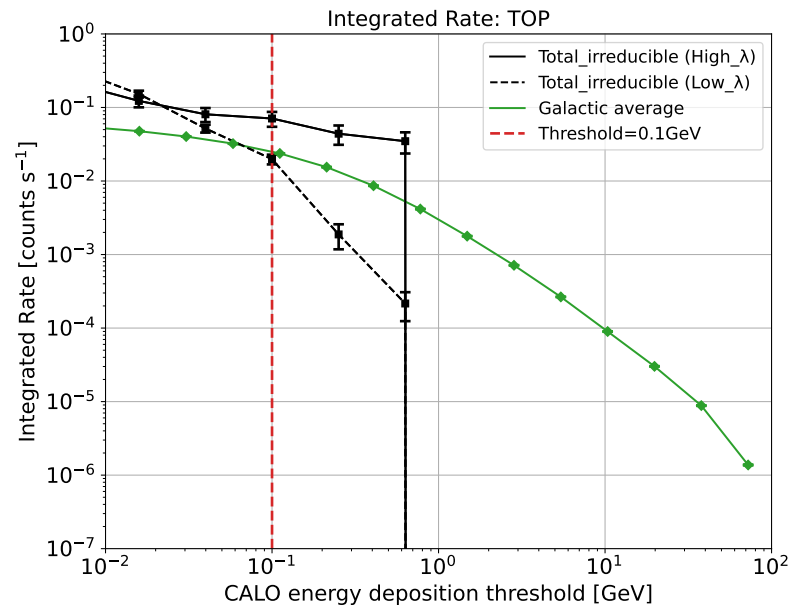


Figure 6. Trigger rates from the irreducible background compared with the rates expected with the diffuse background, as inferred from simulations with a fully hermetic HERD model.

As for the trigger efficiency, we find that the 3IR design is extremely efficient in the energy range we consider, but the PSD veto introduces a loss of efficiency due to backsplash-induced veto, with $\sim 30\%$ ($\sim 70\%$) events being vetoed at ~ 1 GeV (~ 10 GeV) (Figure 7). This could be mitigated by adopting a veto strategy based on a region of interest determined by the combination of modules that produce the trigger. Other HERD triggers provide accessory detection capabilities above ~ 500 MeV and above ~ 15 GeV [9], and the ULEG trigger is designed to attain high efficiency in the lower end of the spectrum.

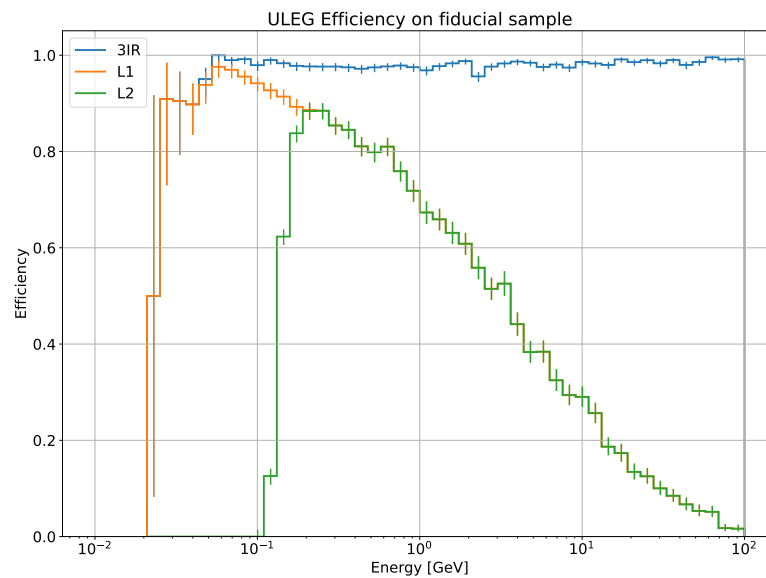


Figure 7. Efficiency of the 3IR, L1 and L2 levels on the fiducial gamma-ray sample.

4. Discussion

We present a preliminary design for the HERD ULEG trigger and its expected performance in the detection of gamma rays in the 100 MeV–100 GeV energy range. The

performance of this design is within the limits imposed by the mission's objectives, but improvements are expected. The final design will feature a region-of-interest- and time-of-flight-based veto strategy. A proof-of-concept version of the hardware implementation of this trigger is undergoing validation at beam tests at PS and SPS at CERN in 2023 and 2024.

Author Contributions: Conceptualization: L.F., K.L., G.L., M.Y., J.B., L.C.-S., O.B., M.M. and J.R.; Data curation: L.F., K.L., G.L., M.Y., J.B., L.C.-S. and J.R.; Formal analysis: L.F., K.L., G.L., M.Y. and J.R.; Investigation: L.F., K.L., G.L., M.Y., J.B. and L.C.-S.; Software: L.F., K.L., G.L., M.Y., J.B. and L.C.-S.; Validation: L.F., K.L., G.L. and M.Y.; Visualization: L.F., K.L., G.L. and M.Y.; Writing—original draft: L.F.; Writing—review & editing: K.L., G.L., M.Y., J.B., L.C.-S., O.B., M.M. and J.R.; Funding acquisition: J.R.; Project administration: J.R.; Supervision: J.R. All authors have read and agreed to the published version of the manuscript.

Funding: This work is supported by Agencia Estatal de Investigación, Ministerio de Ciencia e Investigación: PID2020-116075GB-C22/AEI/10.13039/501100011033, PRE2019-091232, PRE2021-097518; European Union NextGenerationEU: PRTR-C17.I1; Generalitat de Catalunya.

Data Availability Statement: Dataset available on request from the authors

Conflicts of Interest: The authors declare no conflict of interest.

Abbreviations

The following abbreviations are used in this manuscript:

HERD	High Energy cosmic-Radiation Detection facility
CALO	CALORimeter
FIT	Fiber Tracker
PSD	Plastic Scintillation Detector
SCD	Silicon Charge Detector
TRD	Transition Radiation Detector
3IR	Three in a row
RoI	Region of Interest
ULEG	Ultra-Low-Energy Gamma
CSS	Chinese Space Station

Appendix A. The HERD Collaboration

O. Adriani^{1,2}, F. Alemanno^{3,4,a}, C. Altomare⁵, G. Ambrosi⁶, M. Antonelli⁷, P. Azzarello⁸, X.H. Bai⁹, Y.L. Bai⁹, T.W. Bao¹⁰, M. Barbanera⁶, F.C.T. Barbato^{3,4}, F. Bernard¹¹, P. Bernardini^{12,13}, E. Berti², B. Bertucci^{6,14}, P. Betti^{1,2}, X.J. Bi^{10,15}, G. Bigongiari^{16,17}, O. Blanch¹⁸, J. Boix¹⁸, M. Bonghi^{1,2}, V. Bonvicini⁷, S. Bottai², P. Brogi^{16,17}, C. Brugnani^{6,14}, F. Cadoux⁸, I. Cagnoli^{3,4}, H.Y. Cai^{10,15}, D. Campana¹⁹, W.W. Cao⁹, L. Cardiel-Sas¹⁸, J. Casaus²⁰, E. Casilli^{12,13}, R. Catala²¹, E. Catanzani^{6,14}, P.W. Cattaneo²², D. Cerasole^{5,23}, L. Chang²⁴, H. Chen^{10,15}, K. Chen²⁵, L. Chen²⁶, M.L. Chen¹⁰, P.D. Chen²⁷, R. Chen²⁵, Y.D. Cheng^{10,15}, F. Cianetti^{6,14}, A. Comerma²⁸, X.Q. Cong²⁹, P. Coppin⁸, X.Z. Cui¹⁰, R. D'Alessandro^{1,2}, D. D'Urso^{6,30}, C. Díaz²⁰, C. Dai³¹, I. De Mitri^{3,4}, F. de Palma^{12,13}, C. De Vecchi²², V. Di Felice³², A. Di Giovanni^{3,4}, M. Di Santo^{3,4}, L. Di Venere⁵, Y.W. Dong¹⁰, G. Donvito⁵, Y.J. Du³³, M. Duranti⁶, A. Espinosa²¹, K. Fang¹⁰, L. Fariña¹⁸, Y. Favre⁸, H.B. Feng³¹, M. Fernandez Alonso^{3,4}, N. Finetti^{2,34}, G. Fontanella^{3,4}, V. Formato³², J.M. Frieden¹¹, Y. Fu³³, P. Fusco^{5,23}, J.R. Gao⁹, F. Gargano⁵, D. Gascón^{21,35}, D. Gasparrini³², E. Ghose^{12,13,b}, F. Giovacchini²⁰, S. Gómez^{21,28}, K. Gong¹⁰, M.H. Gu¹⁰, D. Guberman²¹, C. Guerrisi^{5,23}, R. Guida³⁶, D.Y. Guo¹⁰, J.H. Guo³⁷, H.L. He^{10,15}, H. Hu¹⁰, H.J. Hu³¹, Y.M. Hu³⁷, Z.X. Hu²⁹, G.S. Huang²⁷, W.H. Huang³⁸, X.T. Huang³⁸, Y.G. Huang³³, M. Ionica⁶, F. Jia³¹, J.S. Jia³³, F. Jiang³¹, X.W. Jiang¹⁰, Y. Jiang^{6,14}, P. Jiao³³, A. Kotenko⁸, D. Kyrtziz^{3,4,c}, D. La Marra⁸, K.R. Lathika¹⁸, L. Li¹⁰, M.J. Li³⁸, M.X. Li²⁵, Q.Y. Li³⁹, Q.Y. Li⁴⁰, R. Li⁹, S.L. Li^{10,15}, T. Li²⁹, T. Li³⁸, X.Q. Li¹⁰, X.Q. Li⁴¹, Y.Y. Li³⁹, Z.H. Li^{10,15}, M.J. Liang^{10,15}, X.Z. Liang⁹, C.L. Liao^{10,15}, F. Licciulli⁵, Y.J. Lin²⁹, B.H. Liu²⁴, D. Liu³⁸, H. Liu²⁶, H.B. Liu³¹, H.W. Liu¹⁰, X. Liu^{10,15}, X.J. Liu¹⁰, X.W. Liu³¹, Y.Q. Liu¹⁰, F. Loparco^{5,23}, S. Loporchio^{5,23}, L. Lorusso^{5,23}, B. Lu¹⁰, R.S. Lu^{10,15}, Y.P. Lu¹⁰, G. Lucchetta¹⁸, J.G. Lv¹⁰, L.W. Lv⁹, P. Maestro^{16,17}, E. Mancini⁶, R. Manera²¹, J. Marin²⁰, P.S. Marrocchesi^{16,17}, G. Marsella^{42,43}, G. Martinez²⁰, M. Martinez¹⁸, J. Mauricio²¹, M.N. Mazziotta⁵, G. Morettini^{6,14}, N. Mori², L. Mussolin^{6,14}, S. Nicotri⁵, Y. Niu³⁸, A. Oliva⁴⁴, D. Orlandi⁴, M. Orta^{21,35}, G. Osteria¹⁹, L. Pacini², B. Panico^{19,45}, F.R. Pantaleo^{5,23}, G. Panzarini^{5,23}, S. Papa³⁶, P. Papini², A. Parenti^{3,4}, M. Pauluzzi^{6,14}, W.X. Peng¹⁰, F. Perfetto¹⁹, C. Perrina¹¹, G. Perrotta³⁶, R. Pillera^{5,23}, A. Pinard¹¹, C. Pizzolotto⁷, S. Qian¹⁰, R. Qiao¹⁰, J.J. Qin⁹, X.B. Qiu²⁹, Z.Y. Qu⁴⁰, Z. Quan¹⁰, A. Rappoldi²², G. Raselli²², F. Renno³⁶, J. Rico¹⁸, M. Rossella²², A. Sanmukh^{21,35}, A. Sanuy^{21,35}, E. Savin⁴⁴, M. Scaringella², V. Scotti^{19,45}, D. Serini⁵, D.L. Shi⁹, Q.Q. Shi³⁸, I. Siddique^{3,4,b}, L. Silveri^{3,4}, G. Silvestre⁶, A. Smirnov^{3,4}, P.G. Song³³, O. Starodubtsev², Y.Z. Su⁴¹, D. Sukhonos⁸, J.Y. Sun^{10,15}, X.L. Sun¹⁰, Z.T. Sun¹⁰, A. Surdo¹³, Z.C. Tang¹⁰, A. Tiberio^{1,2}, A. Tykhonov⁸, V. Vagelli^{6,46}, E. Vannuccini², M. Velasco²⁰, R. Walter⁴⁷, A.Q. Wang³⁸, C. Wang³³, D. Wang²⁵, G.F. Wang²⁷, H. Wang²⁵, J.J. Wang¹⁰, J.W. Wang³³, M. Wang³⁸, R.J. Wang¹⁰, W.S. Wang¹⁰, X.P. Wang⁴¹, Y. Wang³³

Z.G. Wang¹⁰, Z.H. Wang²⁶, J.J. Wei³⁷, P. Wei³¹, Y.F. Wei²⁷, B.B. Wu¹⁰, C. Wu²⁹, L.B. Wu^{3,4,d}, Q. Wu^{10,15}, X. Wu⁸, H.Q. Xie⁴¹, X. Xing⁹, Y.W. Xing³³, M. Xu¹⁰, S.H. Xu⁹, Z.X. Yan^{10,15}, H.B. Yang⁴¹, H.T. Yang^{10,15}, X.G. Yang^{10,15}, Y. Yang³¹, P.F. Yin¹⁰, Y.H. You^{10,15}, M. Yu¹⁸, G. Zampa⁷, N. Zampa⁷, D.L. Zang¹⁰, C. Zhang¹⁰, F. Zhang¹⁰, F.Z. Zhang¹⁰, H.M. Zhang¹⁰, J. Zhang³³, J. Zhang³⁹, S.D. Zhang⁹, S.N. Zhang^{10,15}, X. Zhang³³, X.T. Zhang¹⁰, C.X. Zhao⁴¹, R. Zhao³³, J.K. Zheng⁹, Y.J. Zheng²⁶, F.R. Zhu²⁶, J.Y. Zhu⁴¹, K.J. Zhu¹⁰, L.K. Zou⁴⁰.

¹ Department of Physics, University of Florence, Via Sansone 1, I-50019 Sesto Fiorentino, Firenze, Italy

² Istituto Nazionale di Fisica Nucleare, Sezione di Firenze, Via Sansone 1, I-50019 Sesto Fiorentino, Firenze, Italy

³ Gran Sasso Science Institute (GSSI), Viale Crispi 7, I-67100 L'Aquila, Italy

⁴ Istituto Nazionale di Fisica Nucleare, Laboratori Nazionali del Gran Sasso, Via Acitelli 22, I-67100 Assergi, L'Aquila, Italy

⁵ Istituto Nazionale di Fisica Nucleare, Sezione di Bari, via Orabona 4, I-70126 Bari, Italy

⁶ Istituto Nazionale di Fisica Nucleare, Sezione di Perugia, Via Alessandro Pascoli 23c, I-06123 Perugia, Italy

⁷ Istituto Nazionale di Fisica Nucleare, Sezione di Trieste, via A. Valerio 2, I-34127 Trieste, Italy

⁸ Département de Physique Nucléaire et Corpusculaire (DPNC), Université de Genève, 24 quai Ernest-Ansermet, CH-1211 Genève 4, Switzerland

⁹ Xi'an Institute of Optics and Precision Mechanics of CAS, No.17 Xinxu Road, New Industrial Park, Xi'an Hi-Tech Industrial Development Zone, Xi'an 710019, China

¹⁰ Institute of High Energy Physics, Chinese Academy of Sciences, 19B Yuquan Road, Shijingshan District, Beijing 100049, China

¹¹ Institute of Physics, Ecole Polytechnique Fédérale de Lausanne (EPFL), Bâtiment PH, Station 3, CH-1015 Lausanne, Switzerland

¹² Dipartimento di Matematica e Fisica "E. De Giorgi", Università del Salento, I-73100 Lecce, Italy

¹³ Istituto Nazionale di Fisica Nucleare, Sezione di Lecce, Via per Arnesano, I-73100 Lecce, Italy

¹⁴ Università degli Studi di Perugia, Piazza Università 1, I-06123 Perugia, Italy

¹⁵ University of Chinese Academy of Sciences, No.1 Yanqihu East Rd, Huairou District, Beijing 101408, China

¹⁶ Department of Physical Sciences, Earth and Environment, University of Siena, via Roma 56, I-53100 Siena, Italy

¹⁷ Istituto Nazionale di Fisica Nucleare, Sezione di Pisa, Largo B. Pontecorvo 3, I-56127 Pisa, Italy

¹⁸ Institut de Física d'Altes Energies (IFAE), The Barcelona Institute of Science and Technology (BIST), E-08193 Bellaterra, Barcelona, Spain

¹⁹ Istituto Nazionale di Fisica Nucleare, Sezione di Napoli, Via Cintia, I-80126 Napoli, Italy

²⁰ Centro de Investigaciones Energéticas, Medioambientales y Tecnológicas (CIEMAT), E-28040 Madrid, Spain

²¹ Departament de Física Quàntica i Astrofísica (FQA) and Institut de Ciències del Cosmos (ICCUB), Universitat de Barcelona (UB), E-08028, Barcelona, Spain

²² Istituto Nazionale di Fisica Nucleare, Sezione di Pavia, Via Bassi 6, I-27100 Pavia, Italy

²³ Dipartimento di Fisica "M. Merlin" dell'Università e del Politecnico di Bari, via Amendola 173, I-70126 Bari, Italy

²⁴ North Night Vision Technology Co., Ltd., Hongwai Road 5, Kunming 650217, China

²⁵ PLAC, Key Laboratory of Quark & Lepton Physics (MOE), Central China Normal University, Wuhan 430079, China

²⁶ School of Physical Science and Technology, Southwest Jiaotong University, No.999, Xi'an Road, Chengdu 611756, China

²⁷ Department of Modern Physics, University of Science and Technology of China, Hefei 230026, China

²⁸ Serra Hunter fellow at Polytechnic University of Catalonia (UPC), Electronics Department, E-08019 Barcelona, Spain

²⁹ North Night Vision Science & Technology (Nanjing) Research Institute Co., Ltd, Kangping Street 2, Nanjing 211100, China

³⁰ Università degli Studi di Sassari, Piazza Università 21, I-07100 Sassari, Italy

³¹ Guangxi Key Laboratory for Relativistic Astrophysics, Guangxi University, Daxue East Road 100, Nanning 530004, China

³² Istituto Nazionale di Fisica Nucleare, Sezione di Roma Tor Vergata, via della Ricerca Scientifica 1, I-00133 Roma, Italy

³³ Institute of Special Glass Fiber & Optoelectronic Functional Materials, China Building Materials Academy, Guanzhuang Dongli 1, Chaoyang district, Beijing 100024, China

³⁴ Department of Physical and Chemical Sciences, University of L'Aquila, Via Vetoio, Coppito, I-67100 L'Aquila, Italy

³⁵ Institut d'Estudis Espacials de Catalunya (IEEC), E-08034 Barcelona, Spain

³⁶ Dipartimento di Ingegneria Industriale, Università degli Studi di Napoli Federico II, P.le Tecchio 80, I-80125 Napoli, Italy

³⁷ Purple Mountain Observatory, CAS, No.10 Yuanhua Road, Qixia District, Nanjing 210023, China

³⁸ Shandong University (SDU), 72 Binhai Road, Jimo, Qingdao 266237, China

³⁹ Shandong University (SDU), 27 Shanda Nanlu, Jinan, Shandong 250100, China

⁴⁰ Shandong Institute of Advanced Technology (SDIAT), 1501, Panlong Road, Jinan, Shandong 250100, China

⁴¹ Institute of Modern Physics, CAS, 509 Nanchang Rd., Lanzhou 730000, China

⁴² Dipartimento di Fisica e Chimica "E. Segrè", Università degli Studi di Palermo, via delle Scienze, I-90128 Palermo, Italy

⁴³ Istituto Nazionale di Fisica Nucleare, Sezione di Catania, Via Santa Sofia 64, I-95123 Catania, Italy

⁴⁴ Istituto Nazionale di Fisica Nucleare, Sezione di Bologna, Viale C. Berti Pichat 6/2, I-40127 Bologna, Italy

⁴⁵ Università di Napoli Federico II, Dipartimento di Fisica "Ettore Pancini", Via Cintia, I-80126 Napoli, Italy

⁴⁶ Agenzia Spaziale Italiana, via del Politecnico s.n.c., I-00133 Roma, Italy

⁴⁷ Département d’Astronomie, Université de Genève, Chemin d’Ecogia 16, CH-1290 Versoix, Switzerland

^a Now at Dipartimento di Matematica e Fisica “E. De Giorgi”, Università del Salento, I-73100, Lecce, Italy and Istituto Nazionale di Fisica Nucleare, Sezione di Lecce, Via per Arnesano, I-73100 Lecce, Italy.

^b Also at Dipartimento di Fisica, Università di Trento, via Sommarive 14, I-38123 Trento, Italy.

^c Now at Département de Physique Nucléaire et Corpusculaire (DPNC), Université de Genève, 24 quai Ernest-Ansermet, CH-1211 Genève 4, Switzerland.

^d Now at Institute of Deep Space Sciences, Deep Space Exploration Laboratory, Hefei 230026, China.

References

1. Gargano, F. The High Energy cosmic-Radiation Detection (HERD) facility on board the Chinese Space Station: Hunting for high-energy cosmic rays. In Proceedings of the 37th International Cosmic Ray Conference—PoS (ICRC2021), Berlin, Germany, 15–22 July 2021; p. 26. [\[CrossRef\]](#)
2. Wu, Q. Status of the HERD trigger design. In Proceedings of the 38th International Cosmic Ray Conference (ICRC2023)—Cosmic-Ray Physics (Direct, CRD), Nagoya, Japan, 26 July–3 August 2023; p. 126. [\[CrossRef\]](#)
3. Fariña, L.; Jouvin, L.; Rico, J.; Mori, N.; Gargano, F.; Formato, V.; de Palma, F.; Pizzolotto, C.; Casaus, J.; Mazziota, M.N.; et al. Gamma-ray performance study of the HERD payload. In Proceedings of the 37th International Cosmic Ray Conference (ICRC2021)—GAD—Gamma Ray Direct, Berlin, Germany, 15–22 July 2021; p. 651. [\[CrossRef\]](#)
4. Liu, X.; Adriani, O.; Bai, X.H.; Bai, Y.L.; Bao, T.W.; Berti, E.; Betti, P.; Bottai, S.; Cao, W.W.; Casaus, J.; et al. Double read-out system for the calorimeter of the HERD experiment. In Proceedings of the 38th International Cosmic Ray Conference (ICRC2023)—Cosmic-Ray Physics (Direct, CRD), Nagoya, Japan, 26 July–3 August 2023; p. 97. [\[CrossRef\]](#)
5. Mori, N. GGS: A Generic Geant4 Simulation package for small- and medium-sized particle detection experiments. *Nucl. Instrum. Methods Phys. Res. Sect. A Accel. Spectrometers Detect. Assoc. Equip.* **2021**, *1002*, 165298. [\[CrossRef\]](#)
6. Agostinelli, S.; Allison, J.; Amako, K.; Apostolakis, J.; Araujo, H.; Arce, P.; Asai, M.; Axen, D.; Banerjee, S.; Barrand, G.; et al. Geant4—A simulation toolkit. *Nucl. Instrum. Methods Phys. Res. Sect. A Accel. Spectrometers Detect. Assoc. Equip.* **2003**, *506*, 250–303. [\[CrossRef\]](#)
7. Lucchetta, G.; Fariña, L.; Yu, M.; Lathika, K.R.; Rico, J.; Cardiel, L.; Boix, J.; Martínez, M.; Casaus, J.; Mauricio, J.; et al. Gamma-ray performance of the High Energy cosmic-Radiation Detection (HERD) space mission. In Proceedings of the 38th International Cosmic Ray Conference (ICRC2023)—Gamma-ray Astronomy (GA), Nagoya, Japan, 26 July–3 August 2023; p. 691. [\[CrossRef\]](#)
8. Ackermann, M.; Ajello, M.; Albert, A.; Allafort, A.; Atwood, W.B.; Axelsson, M.; Baldini, L.; Ballet, J.; Barbiellini, G.; Bastieri, D. The Fermi Large Area Telescope On Orbit: Event Classification, Instrument Response Functions, and Calibration. *Astrophys. J. Suppl.* **2012**, *203*, 4. [\[CrossRef\]](#)
9. Velasco Frutos, M.A.; Bao, T.; Berti, E.; Bonvicini, V.; Casaus, J.; Giovacchini, F.; Liu, X.; Marco, R.; Marín, J.; Martínez, G.; et al. The High Energy cosmic Radiation Detector (HERD) Trigger System. In Proceedings of the 37th International Cosmic Ray Conference (ICRC2021)—CRD—Cosmic Ray Direct, Berlin, Germany, 15–22 July 2021; p. 62. [\[CrossRef\]](#)

Disclaimer/Publisher’s Note: The statements, opinions and data contained in all publications are solely those of the individual author(s) and contributor(s) and not of MDPI and/or the editor(s). MDPI and/or the editor(s) disclaim responsibility for any injury to people or property resulting from any ideas, methods, instructions or products referred to in the content.